J. Fluid Mech. (1987), *vol.* 174, *pp.* 135–153
Printed in Great Britain

Buoyancy-driven crack propagation: a mechanism for magma migration

By D. A. SPENCE,
Department of Mathematics, Imperial College, London, SW7 2BZ, UK

P. W. SHARP
Department of Computer Science, University of Toronto, Toronto M5S 1A4, Canada

AND D. L. TURCOTTE
Department of Geological Sciences, Cornell University, Ithaca, NY 14853, USA

(Received 10 October 1985 and in revised form 15 May 1986)

A solution has been obtained for steady propagation of a two-dimensional fluid fracture driven by buoyancy in an elastic medium. The problem is formulated in terms of an integro-differential equation governing the elastic deformation, coupled with the differential equation of lubrication theory for viscous flow in the crack. The numerical treatment of this system is carried out in terms of an eigenfunction expansion of the cavity shape, in which the coefficients are found by use of a nonlinear constrained optimization technique. When suitably non-dimensionalized, the solution appears to be unique. It exhibits a semi-infinite crack of constant width following the propagating fracture. For each value of the stress intensity factor of the medium, the width and propagation speed are determined. The results are applied to the problem of the vertical ascent of magma through the earth's mantle and crust. Values obtained for the crack width and ascent velocity are in accord with observations. This mechanism can explain the high ascent velocities required to quench diamonds during a Kimberlite eruption. The mechanism can also explain how basaltic eruptions can carry large mantle rocks (xenoliths) to the surface.

1. Introduction

Fluid fracture is accepted as an important mechanism for the transport of magmas in the Earth's crust and mantle. Evidence for fluid fracture comes from studies of the structure and emplacement of dykes and sills (Pollard 1973, 1976; Pollard & Muller 1976; Delaney & Pollard 1981, 1982; Shaw 1980; Muller & Muller 1980). The vertical transport of magmas is driven by the differential buoyancy of the magma relative to the country rock. Buoyancy-driven fluid fractures as a mechanism for magma migration have been studied by Weertman (1971), Anderson & Grew (1977), Secor & Pollard (1975), and Stevenson (1982). One of the most spectacular examples of buoyancy-driven magma fracture is the Kimberlite eruption responsible for the emplacement of diamonds at the earth's surface (Anderson 1979). These eruptions require high velocities in order to quench diamonds; the required velocities are estimated to be in the range 0.5–5 m/s (Pasteris 1984).

Spence & Sharp (1985) obtained a series of similarity solutions for pressure-driven fluid fracture. These results were applied to the emplacement of dykes and sills by Spence & Turcotte (1985) and Emerman, Turcotte & Spence (1986). These solutions

treat the elastic deformation of the host medium together with the fluid-transport problem, and take account of the fracture resistance of the medium through a stress-intensity factor. Both two-dimensional and axisymmetric flows were considered. The lubrication approximation was used and both laminar and turbulent flows were considered. In this paper the approach is extended to buoyancy-driven fluid fracture.

The problem is formulated in §2. The governing elastic and lubrication equations for a steadily advancing crack are then combined into a single nonlinear integral equation in §3, and some of the properties of its solution are investigated analytically. The numerical method of solution chosen is presented in §4. It involves expansion of the shape function h in terms of Chebychev polynomials with unknown coefficients. These coefficients were determined by a constrained optimization technique described in §5, leading to a solution which appears to be unique. Parameters obtained from this solution are used in §6 to discuss magma transport in the crust.

2. Formulation of the problem

A vertically-propagating two-dimensional crack is considered. The crack is embedded in a uniform impermeable elastic medium with shear modulus μ, Poisson's ratio ν, and density ρ_s representing the surrounding rock. The crack width is $2h(y,t)$ (y measured vertically upwards) and we assume that the walls are almost parallel in the sense that the lengthscale over which h changes significantly is large in comparison with $\mu/\rho_s g$. Then if Q is the upward flux of fluid in the crack, continuity requires

$$\frac{\partial}{\partial t}(2h)+\frac{\partial Q}{\partial y}=0. \tag{2.1}$$

Provided the crack is sufficiently thin and the fluid viscosity η_m sufficiently large, the flow will be laminar and may be treated by lubrication theory. Q is the flux induced by the external pressure gradient together with the hydrostatic pressure $-\rho_m g y$, ρ_m being the density of the fluid magma contained within the crack:

$$Q=-\frac{2h^3}{3\eta_m}\left(\frac{\partial p}{\partial y}+\rho_m g\right). \tag{2.2}$$

The pressure acting on the walls of the crack is

$$p=-\rho_s g y+p_0(y,t), \tag{2.3}$$

where $p_0(y,t)$ is the non-hydrostatic part of the stress tensor, i.e. σ_{11} if suffix 1 indicates the horizontal direction, and represents the elastic contribution to the pressure, which is given in terms of the distribution of h by

$$p_0(y,t)=-\left(\frac{\mu}{1-\nu}\right)\frac{1}{\pi}\int_{-\infty}^{\infty}\frac{\partial h(\eta,t)}{\partial \eta}\frac{\mathrm{d}\eta}{\eta-y} \tag{2.4}$$

(the integral in (2.4) is a Cauchy principal value).

Equations (2.1)–(2.3) combine to give the Reynolds equation

$$\frac{\partial h}{\partial t}=\frac{1}{3\eta_m}\frac{\partial}{\partial y}\left[h^3\left(\frac{\partial p_0}{\partial y}-g\Delta\rho\right)\right], \tag{2.5}$$

where

$$\Delta\rho=\rho_s-\rho_m \tag{2.6}$$

is the density difference driving the buoyancy force. We seek solutions of (2.4) and (2.5) for cracks that propagate at a constant speed c. Thus we require

$$h = h(z), \quad p_0 = p_0(z) \quad \text{where } z = ct - y. \tag{2.7}$$

Then (2.5) becomes

$$c\frac{\mathrm{d}h}{\mathrm{d}z} = \frac{1}{3\eta_\mathrm{m}}\frac{\mathrm{d}}{\mathrm{d}z}\left[h^3\left(\frac{\mathrm{d}p_0}{\mathrm{d}z} + g\Delta\rho\right)\right], \tag{2.8}$$

and integration gives

$$3\eta_\mathrm{m} ch - h^3\left(\frac{\mathrm{d}p_0}{\mathrm{d}z} + g\Delta\rho\right) = 0, \tag{2.9}$$

where the condition $h(-\infty) = 0$ has been used to set the constant of integration to zero. Since the elastic pressure gradient $\mathrm{d}p_0/\mathrm{d}z$ must vanish far from the crack tip, i.e. as $z \to \infty$, the speed of propagation is related to the limiting crack width by

$$c = \left(\frac{g\Delta\rho}{3\eta_\mathrm{m}}\right)h^2(\infty). \tag{2.10}$$

Also (2.4) becomes

$$p_0(z) = -\left(\frac{\mu}{1-\nu}\right)\frac{1}{\pi}\int_0^\infty \frac{\mathrm{d}h(\xi)}{\mathrm{d}\xi}\frac{\mathrm{d}\xi}{\xi - z}, \tag{2.11}$$

the lower limit of integration now being the crack tip $z = 0$. It is convenient to introduce the length- and time-scales

$$L = \frac{\mu}{(1-\nu)g\Delta\rho}, \quad T = 3\eta_\mathrm{m}\left(\frac{1-\nu}{\mu}\right). \tag{2.12}$$

Then if we replace z, h and p_0 by dimensionless quantities x, $\bar{h}$, $\bar{p}$ defined in terms of L and the crack width $h(\infty) = h_\infty$, by writing

$$\left.\begin{aligned} z &= (Lh_\infty)^{\frac{1}{2}}x, \quad h(z) = h_\infty \bar{h}(x), \\ p_0(z) &= \left(\frac{\mu}{1-\nu}\right)\left(\frac{h_\infty}{L}\right)^{\frac{1}{2}}\bar{p}(x), \end{aligned}\right\} \tag{2.13}$$

the speed of propagation is

$$c = \frac{h_\infty^2}{LT}, \tag{2.14}$$

while (2.9) and (2.11) become

$$\bar{h}^2\left(\frac{\mathrm{d}\bar{p}}{\mathrm{d}x} + 1\right) = 1, \tag{2.15}$$

$$\bar{p}(x) = -\left(\frac{1}{\pi}\right)\int_0^\infty \frac{\mathrm{d}\bar{h}(s)}{\mathrm{d}s}\frac{\mathrm{d}s}{s - x}. \tag{2.16}$$

These are the equations treated analytically in §3 and numerically in §§4 and 5.

2.1. *Stress singularity at crack tip*

We next relate the stress singularity at the crack tip to the stress-intensity factor K through

$$-p(y,t) \sim \frac{K}{[2(y-y_0)]^{\frac{1}{2}}}, \tag{2.17}$$

as y approaches the crack tip $y_0(t)$ from outside. In terms of a non-dimensional stress-intensity factor $\gamma = (1-\nu)K/L^{\frac{1}{2}}\mu$, (2.17) becomes

$$-\bar{p}(x) \approx \frac{\lambda}{(-x)^{\frac{1}{2}}}, \tag{2.18}$$

where

$$\lambda = 2^{\frac{1}{2}}\gamma\left(\frac{L}{h_\infty}\right)^{\frac{3}{4}}. \tag{2.19}$$

This limiting behaviour requires that the crack shape near the tip should be given by

$$\bar{h} \doteqdot 2\lambda x^{\frac{1}{2}} \quad \text{near } x = 0. \tag{2.20}$$

For a specified value of γ the width h_∞ is related to λ by (2.19), and since the speed of propagation c is given in terms of h_∞ by (2.14), it is also related to λ. One of the questions we must address ourselves to is whether the set of equations (2.15), (2.16) has a solution exhibiting the limiting behaviour given by (2.20) for all values of λ, for a discrete set of values, or for a single value.

3. The integral equation for cavity shape

In this section the elasticity equation (2.16) will be combined with the lubrication equation (2.15) to yield a single integral equation for $\bar{h}(x)$, and the limiting behaviour of the solution for small and for large values of x derived. From now on we will omit the bars over h and p, so write the equations as

$$p(x) = -\frac{1}{\pi}\int_0^\infty \frac{h'(s)\,\mathrm{d}s}{s-x}, \tag{3.1}$$

$$p'(x) = \frac{1}{h^2(x)} - 1, \tag{3.2}$$

and the solution is to be constrained so that

$$h > 0 \quad \text{for all } x > 0, \quad h(0) = 0, \quad h(\infty) = 1. \tag{3.3}$$

Inversion of (3.1) on the interval $(0, \infty)$ gives

$$h'(x) = \left(\frac{1}{\pi}\right)\int_0^\infty \left(\frac{s}{x}\right)^{\frac{1}{2}} \frac{p(s)\,\mathrm{d}s}{s-x} + \frac{C}{x^{\frac{1}{2}}},$$

where C is an arbitrary constant. For solutions in which h is bounded as $x \to \infty$ we must exclude the possibility that $h' \approx x^{-\frac{1}{2}}$, and therefore take $C = 0$. The equation can then be integrated with respect to x to give

$$h(x) = \left(\frac{1}{\pi}\right)\int_0^\infty \ln\left|\frac{x^{\frac{1}{2}}+s^{\frac{1}{2}}}{x^{\frac{1}{2}}-s^{\frac{1}{2}}}\right| p(s)\,\mathrm{d}s,$$

and integration by parts on the right-hand side converts this to

$$h(x) = \left(\frac{1}{\pi}\right)\int_0^\infty k(x,s)\,p'(s)\,\mathrm{d}s, \tag{3.4}$$

with

$$k(x,s) = (x-s)\ln\left|\frac{x^{\frac{1}{2}}+s^{\frac{1}{2}}}{x^{\frac{1}{2}}-s^{\frac{1}{2}}}\right| - 2(xs)^{\frac{1}{2}}.$$

Thus h satisfies the nonlinear integral equation

$$h(x) = \left(\frac{1}{\pi}\right)\int_0^\infty k(x,s)\left(\frac{1}{h^2(s)} - 1\right)\mathrm{d}s, \tag{3.5}$$

on the interval $(0, \infty)$. Before the expansion procedure for numerical solution is developed, some properties of the solution (if any) may be noted.

Firstly, the limiting behaviour for small x is given by that of the kernel, which is

$$k(x,s) \approx -4(xs)^{\frac{1}{2}} \quad \left(\frac{x}{s} \ll 1\right).$$

From this it follows that for small values of x

$$h(x) \approx 2\lambda x^{\frac{1}{2}}, \quad \text{where } \lambda = -\frac{2}{\pi}\int_0^\infty s^{\frac{1}{2}}p'(s)\,\mathrm{d}s,$$

and therefore, by (3.2), $p'(x) \sim 1/4\lambda^2 x$ as $x \to 0$. This leads via (3.1) to a further term for small x:

$$h(x) = 2\lambda x^{\frac{1}{2}} + \left(\frac{\pi}{4\lambda^2}\right)x + \ldots. \tag{3.6}$$

λ is related to the stress-intensity factor at the crack tip $x = 0$, since if $h'(s) \approx \lambda s^{-\frac{1}{2}}$ near $s = 0$, then it follows from (3.1) that

$$p(x) \sim -\frac{\lambda}{(-x)^{\frac{1}{2}}}, \tag{3.7}$$

as $x \to 0$ from the left. A quadratic relationship between λ and h can be obtained by multiplying (3.4) on both sides by $p'(x)$ and integrating for 0 to ∞. This gives

$$\int_0^\infty p'(x)\,h(x)\,\mathrm{d}x = \frac{1}{\pi}\int_0^\infty p'(x)\,\mathrm{d}x\int_0^\infty (x-s)\,\ln|\,|\,p'(s)\,\mathrm{d}s$$
$$-\frac{2}{\pi}\int_0^\infty p'(x)\,\mathrm{d}x\int_0^\infty (xs)^{\frac{1}{2}}p'(s)\,\mathrm{d}s.$$

The first integral on the right is identically zero, since its kernel is an antisymmetric bounded function of x and s. Therefore

$$\int_0^\infty p'(x)\,h(x)\,\mathrm{d}x = -\frac{2}{\pi}\left(\int_0^\infty x^{\frac{1}{2}}p'(x)\,\mathrm{d}x\right)^2 = -\tfrac{1}{2}\pi\lambda^2. \tag{3.8}$$

(This result can also be derived directly from (3.1) using properties of singular integrals.) The relationship

$$\int_0^\infty \left(h - \frac{1}{h}\right)\mathrm{d}s = \tfrac{1}{2}\pi\lambda^2, \tag{3.9a}$$

which holds when p' is given by (3.2), provides a numerical check on the accuracy of the solution of the combined system. Another check is provided by the inequality

$$2\int_0^\infty (h-1)\,\mathrm{d}s \geqslant \tfrac{1}{2}\pi\lambda^2, \tag{3.9b}$$

which follows by adding the positive quantity

$$\int_0^\infty (h^{\frac{1}{2}} - 1/h^{\frac{1}{2}})^2\,\mathrm{d}s$$

to both sides of (3.9a).

Secondly, the asymptotic behaviour of h for large x can be inferred by writing (3.1) as

$$p(x) = \left(\frac{1}{\pi}\right)\int_0^\infty \left(\frac{1}{x}+\frac{s}{x^2}\right)h'(s)\,\mathrm{d}s - \frac{1}{\pi x^2}\int_0^\infty \frac{s^2 h'(s)\,\mathrm{d}s}{s-x} \equiv \frac{1}{\pi x} - \frac{A}{\pi x^2} - R(x), \tag{3.10}$$

say, where

$$A = -\int_0^\infty s h'(s)\,\mathrm{d}s = \int_0^\infty (h(s)-1)\,\mathrm{d}s.$$

Therefore as $x \to \infty$, $p'(x) \approx -(1/\pi x^2)$, so that by (3.2)

$$h(x) \approx 1 + \frac{1}{2\pi x^2}. \tag{3.11}$$

This behaviour makes it possible to evaluate further terms: in Appendix A we find

$$R(x) = \frac{\ln x + 2\pi B - \frac{1}{2}}{\pi^2 x^3} + O\left(\frac{1}{x^3}\right),$$

where

$$B = \int_0^\infty s\left(h(s) - 1 - \frac{1}{2\pi(s^2+1)}\right)\mathrm{d}s,$$

and the series for h can be extended to terms of order x^{-4}:

$$h(x) \sim 1 + \frac{1}{2\pi x^2} - \frac{A}{\pi x^3} - \frac{3(\ln x + 2\pi B) - \frac{13}{4}}{2\pi^2 x^4} + \ldots. \tag{3.12}$$

4. Scheme for numerical solution

To solve the integral equation numerically, we have interpolated $p'(x)$ in the form of a Chebychev series:

$$p'^{(N)}(x) = [x(x+1)]^{-1} \sum_{n=0}^{N} A_n T_n\left(\frac{1-x}{1+x}\right). \tag{4.1}$$

This form was chosen (a) because it possesses the required limiting behaviour, with $p' \approx x^{-1}$ near $x = 0$, and $p' \approx x^{-2}$ as $x \to \infty$, and (b) because when it is substituted into (3.4), the resulting integrals

$$H_n(x) = \left(\frac{1}{\pi}\right)\int_0^\infty k(x,s)[s(s+1)]^{-1} T_n\left(\frac{1-s}{1+s}\right)\mathrm{d}s, \tag{4.2}$$

can be evaluated in closed form, so that the left-hand side is approximated by

$$h^{(N)}(x) = \sum_{n=0}^{N} A_n H_n(x). \tag{4.3}$$

We then chose the coefficients A_n in this expansion to ensure that $p'^{(N)}$ was related to $h^{(N)}$ in accordance with (3.2), by minimizing the sum

$$F(M,N) = \sum_{i=1}^{M} [p'(x_i)^{(N)} - (h(x_i)^{(N)})^{-2} + 1]^2, \tag{4.4}$$

over a chosen set of M points $x_1 \ldots x_M$. The details are presented in §5. With M, N of order 100 it is possible to reduce F to the order of 10^{-15}.

4.1. *Expressions for* H_n

It is convenient to introduce a trigonometrical variable ψ by means of

$$x = \tan^2(\tfrac{1}{2}\psi), \tag{4.5}$$

so mapping the flow region $(0, \infty)$ onto $(0, \pi)$. Then $H_n(x)$ becomes

$$H_n(\psi) = \left(\frac{1}{\pi}\right)(\sec^2 \tfrac{1}{2}\psi) \int_0^\pi \left(\frac{\cos\theta - \cos\psi}{\sin\theta}\right) \ln\left|\frac{\tan\frac{1}{2}\psi + \tan\frac{1}{2}\theta}{\tan\frac{1}{2}\psi - \tan\frac{1}{2}\theta}\right| (\cos n\theta)\, \mathrm{d}\theta$$
$$- 2(\tan\tfrac{1}{2}\psi)\, \delta(n, 0). \quad (4.6)$$

These integrals are evaluated in Appendix B. The first three are

$$\left.\begin{aligned} H_0 &= (\pi - \psi)\tan^2\tfrac{1}{2}\psi - \psi - 2\tan\tfrac{1}{2}\psi, \\ H_1 &= H_0 + 2\psi, \\ H_2 &= H_0 + \sin\psi, \end{aligned}\right\} \quad (4.7)$$

and the remainder are given by the recurrence relations

$$H_{n+1} - H_{n-1} = (n\cos^2\tfrac{1}{2}\psi)^{-1}\left\{\frac{\sin(n+1)\psi}{n+1} - \frac{\sin(n-1)\psi}{n-1}\right\} \quad (n = 2, 3, \ldots). \quad (4.8)$$

In terms of x, the leading terms are

$$\left.\begin{aligned} H_0 &= -2(x^{\frac{1}{2}} + (1+x)\tan^{-1}x^{\frac{1}{2}}) + \pi x, \\ &= -4x^{\frac{1}{2}} + \pi x + O(x^{\frac{3}{2}}) \quad \text{near } x = 0, \\ H_1 &= H_0 + 4\tan^{-1}x^{\frac{1}{2}} = \pi x + O(x^{\frac{3}{2}}) \quad \text{near } x = 0, \\ H_2 &= H_0 + \frac{4x^{\frac{1}{2}}}{(1+x)} = \pi x + O(x^{\frac{3}{2}}) \quad \text{near } x = 0. \end{aligned}\right\} \quad (4.9)$$

The recurrence relation shows that $H_{n+1} - H_{n-1} = O(x^{\frac{3}{2}})$ near $x = 0$ so that $H_n = \pi x + O(x^{\frac{3}{2}})$ near $x = 0$ for $n = 1, 2, 3 \ldots$. Hence the limiting behaviour of H as calculated from (4.3) is

$$H(x) = -4A_0 x^{\frac{1}{2}} + \pi x\left(\sum_{n=0}^{N} A_n\right) + O(x^{\frac{3}{2}}),$$

showing that the coefficient of the singularity at $x = 0$ is given by

$$\lambda = -2A_0, \quad (4.10)$$

and that to comply with (3.6) we must have

$$\sum_{n=0}^{N} A_n = \frac{1}{16A_0^2}. \quad (4.11)$$

This provides a check on the numerical results. Further checks are provided by consideration of the asymptotic form of $h(x)$ as given by (3.12). For $x \gg 1$ the expressions (4.9) show that

$$H_0 \approx -\pi + \frac{4}{3x^{\frac{1}{2}}}, \quad H_1 \approx \pi - \frac{8}{3x^{\frac{1}{2}}}, \quad H_2 \approx -\pi + \frac{16}{3x^{\frac{1}{2}}},$$

and more generally, the recurrence relation gives

$$H_{n+1} - H_{n-1} \approx (-1)^{n-1}\frac{16}{3x^{\frac{1}{2}}},$$

whence

$$H_n \approx (-1)^{n-1}\left(\pi - \frac{8n}{3x^{\frac{1}{2}}}\right) \quad \text{for } n = 1, 2, 3 \ldots. \quad (4.12)$$

Therefore the sum (3.15) is asymptotically

$$-\sum_{n=0}^{N}(-1)^n A_n+\frac{8}{3x^{\frac{1}{2}}}(\tfrac{1}{2}A_0-A_1+2A_2-\ldots)+O(x^{\frac{3}{2}}).$$

Comparison with (3.13) shows that we must have

$$\Sigma(-1)^n A_n=-\frac{1}{\pi}, \tag{4.13}$$

$$\tfrac{1}{2}A_0+\Sigma(-1)^n nA_n=0. \tag{4.14}$$

A further identity comes from the asymptotic form of p'. For large x,

$$T_n\left(\frac{1-x}{1+x}\right)\approx(-1)^n\left(1-\frac{2n^2}{x}\right),$$

whence from (4.1),

$$p'(x)\approx\frac{1}{x^2}\Sigma(-1)^n A_n\left(1-\frac{2n^2+1}{x}\right).$$

Identifying this with the first two terms of the expansion (3.10), which on differentiation yields

$$p'(x)\approx-\frac{1}{\pi x^2}+\frac{2A}{\pi x^3},$$

we see that the leading terms are the same when (4.13) holds, while the $1/x^3$ terms give

$$A=\int_0^\infty(h-1)\,\mathrm{d}x=\tfrac{1}{2}-\pi\Sigma(-1)^n n^2 A_n. \tag{4.15}$$

This provides a check on the solution since the constant A can be evaluated directly by quadrature.

5. Numerical procedure and results

As outlined in the last section, the approach adopted to the solution of the integral equation (4.4) was to seek a vector of coefficients $A^{(N)}$ characterizing the interpolations $h^{(N)}$, $p'^{(N)}$ by minimizing the objective function $F(M,N)$ (equation (4.4)) subject to the constraints (3.3) applied to $h^{(N)}$, i.e. for suitably chosen M, N

$$\text{find } \min_{A^{(N)}} F(M,N), \quad \text{subject to } h^{(N)}>0. \tag{5.1a, b}$$

The solution would be acceptable if the minimum of F was sufficiently small, and if the identities and limiting properties derived in §§3, and 4, namely

$$h=-4A_0 s^{\frac{1}{2}} \quad (x\ll 1), \quad h\approx 1+\frac{1}{\pi x^2}\left(\frac{1}{2}-\frac{A}{x}\right), \tag{5.1c, d}$$

$$\Sigma(-1)^i A_i=-\frac{1}{\pi}, \quad \Sigma A_i=\frac{1}{16A_0^2}, \tag{5.1e, f}$$

$$\int_0^\infty(h-1)\,\mathrm{d}x=\tfrac{1}{2}-\pi\Sigma(-1)^i i^2 A_i, \tag{5.1g}$$

$$\int_0^\infty\left(h-\frac{1}{h}\right)\mathrm{d}x=-2\pi A_0^2, \tag{5.1h}$$

$$\tfrac{1}{2}A_0+\Sigma(-1)^i iA_i=0, \tag{5.1i}$$

were satisfied to a prescribed accuracy.

Clearly $F(M, N)$ possesses a minimum for each M and N. The question is whether values of M and N can be found such that the minimum is sufficiently small to ensure the identities (5.1$c-i$) are satisfied to the prescribed accuracy. For this to occur it is necessary for errors resulting from truncation of (4.3) to be small. Before using these identities to check a solution to (5.1a, b) we required F to be small (less than 10^{-6}), A_N to be small and the A_i to change little when (5.1a, b) is resolved with larger N.

Problem (5.1) was solved using a scheme based on the continuation method given in Spence & Sharp (1985) which involved using M, N and the mesh as the continuation parameters. To apply this approach to the current problem it was necessary to replace the interval of integration $[0, \infty]$ by a finite interval $[0, x_m]$ and to choose the mesh so that the height was resolved sufficiently for both small and large values of x and in the neighbourhood of the expected maximum near $x = 1$.

For given values of M, N and a given mesh the constrained nonlinear least-squares problem (5.1a, b) was solved using the Harwell routine VEOIAD. Two tests for convergence are used. One is

$$|A_j^{i+1} - A_j^i| < \epsilon \quad (j = 0, \ldots, N),$$

and the other is

$$F(A_0^{i+1}, A_1^{i+1}, \ldots, A_N^{i+1}) = F(A_0^i, A_1^i, \ldots, A_N^i),$$

where A_i^i is the value of A_j at the ith iteration and ϵ_j is the error tolerance. For the solutions presented here ϵ_j was generally set to 10^{-9} except for checks of the solution when $\epsilon_j = 10^{-10}$, 10^{-11}.

Initial calculations were performed with $x_M = 100$ and a uniform mesh in x.

$$x_i = \frac{ix_M}{M} \quad (i = 1, \ldots, M).$$

The intention was to increase M, N and x_M until the solution to problem (5.1) was known to the prescribed accuracy. However, the results for small M ($\leqslant 30$) showed that this would require a prohibitively large M. After some experimentation a uniform mesh in θ was adopted:

$$\theta_i = \frac{i\pi}{M+1} \quad (i = 1, \ldots, M),$$

satisfying qualitatively the mesh requirements.

M and N were increased in small increments until $M = 100$ and $N = 49$ for which F was 1.2×10^{-4}. We then attempted to reduce F below 10^{-6} by increasing M to 110 and N to 54. But F decreased only to 1.1×10^{-4}.

Instead of increasing M further with $N < \frac{1}{2}M$ we set $N = M-1$ making problem (5.1a, b) a system of M equations in M unknowns with M constraints. One disadvantage of this approach is that standard results in approximation theory show that increasing the ratio N/M will in general lead to high frequency oscillations in $h^{(N)}$ and $p'^{(N)}$. However, as seen below these had little effect on the solution.

To solve problem (5.1) with $N = M-1$ we had to repeat the continuation on M and N because the solutions already obtained with the extra A_i suitably extrapolated were not sufficiently accurate initial estimates. We started with $M = 5$, $N = 4$ for which the minimization was easily achieved. Next M and N were increased in unit steps to 20 and then m larger steps until $M = 110$, $N = 109$ for which F was 1.1×10^{-15}, $A_0 = -0.65391654$ and $A_{109} = 1.5 \times 10^{-7}$. Although this was an acceptable solution of problem (5.1) we sought greater accuracy by increasing M up to 200. It

i	x_1	$h^{(N)}$ (equation (4.3))	$-4A_0 x^{\frac{1}{2}} + (\pi/16A_0^2)\,x$
1	0.00001	0.0256	0.0256
5	0.00238	0.1286	0.1288
9	0.00775	0.2329	0.2338
13	0.01626	0.3382	0.3410
17	0.02802	0.4443	0.4507
21	0.04318	0.5512	0.5634
25	0.06194	0.6587	0.6794
29	0.08453	0.7665	0.7993

TABLE 1. Computed values of h for small x compared with limiting expression (3.6) ($M = 160$, $N = 159$, $\epsilon_j = 10^{-9}$, $A_0 = -0.653916$)

i	x_i	$h-1$ (computed using $A^{(N)}$, equation (4.3))	$h-1$ (asymptotic, four-term, equation (3.12))
118	5.03	$-0.3821, -1$	$-0.2480, -2$
124	7.02	$-0.2633, -4$	$0.4397, -3$
130	10.27	$0.7338, -3$	$0.7315, -3$
136	16.15	$0.4397, -3$	$0.4338, -3$
142	28.44	$0.1687, -3$	$0.1678, -3$
148	61.50	$0.3950, -4$	$0.3946, -4$
154	213.7	$0.34255, -5$	$0.34252, -5$
160	10505	$0.14410, -8$	$0.14418, -8$

TABLE 2. Comparison of computed values of h with asymptotic expansion ($M = 160$, $N = 159$, $\epsilon_j = 10^{-9}$. The constants in the expansion are $A = 1.7578$, $B = 2.84$)

was found for M greater than 160 that the gain in accuracy did not justify the extra computational cost.

With $M = 160, N = 159, F$ was 4.2×10^{-16}, A_0 was $-0.653915\,76$ and the coefficients decreased uniformly so that A_{50}, A_{100} and A_{150} were respectively 0.145×10^{-2}, 0.166×10^{-5} and 0.130×10^{-7}. A_{159} was 2.4×10^{-10}. Values of h for small x and for large x are listed and compared with the appropriate limiting formulae in tables 1 and 2. We have also included a summary of the agreement with the identities $(5e-i)$ in table 3. In all tables the results are displayed in exponent form, i.e. $a, -b \equiv a \times 10^{-b}$.

Tables 1 and 2 illustrate striking agreement with the theoretical estimates of $(5.1\,c, d)$. From table 3, identity $(5.1\,e)$ which ensures $h^N(\infty) = 1$ is seen to be satisfied with very high accuracy. This is consistent with the accuracy of the asymptotic solution shown in table 2. The remaining identities contain relative discrepancies of order 10^{-3} or less. The integrals involved in this table, namely

$$A = \int_0^\infty (h-1)\,\mathrm{d}x, \quad (\text{in } 5.1\,g)$$

and

$$\int_0^\infty \left(h - \frac{1}{h}\right)\mathrm{d}x \quad (\text{in } 5.1\,h),$$

were calculated by Romberg integration from 0 to x_m and analytic integration using

Relation	Left-hand side	Right-hand side	Ratio (l/r)
(5.1*e*)	−0.318310	−0.318310	1
(5.1*f*)	0.1459	0.1461	0.9983
(5.1*g*)	1.758	1.748	1.006
(5.1*h*)	−2.686594	−2.686727	1.00005
(5.1*i*)	1.9, −5	0	—

The integrals A and B (equations (3.10), (3.12)) are $A = 1.7578$, $B = 2.84$.

TABLE 3. Summary of numerical identities ($M = 160$, $N = 159$, $\epsilon_j = 10^{-9}$)

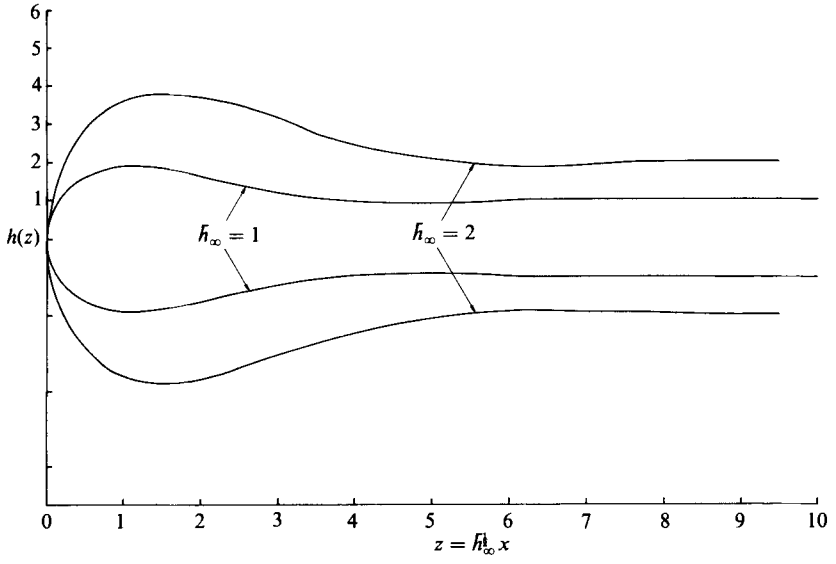

FIGURE 1. Shape of the propagating fluid fracture in terms of the non-dimensional variables.

the asymptotic form for h from x_m to ∞. For the second integral the lower integration limit was replaced by δ ($0 < \delta \ll x_1$) to avoid computational difficulties at the singularity.

Three important issues related to the numerical results are (i) the uniqueness of the solution to (5.1*a*, *b*), (ii) their dependence on M and the form of the objective function, and (iii) the accuracy of the integration scheme.

When solving (5.1) we assumed that while F may possess several local minima, the global minimum was required in order to make F sufficiently small. Because the routine VEOIAD does not necessarily find the global minimum the nature of the computed minimum must be assessed using indirect methods which involve searching for other minima. We resolved problem (4.1) using different initial estimates, more severe error tolerances and with round-off error controls incorporated. Despite extensive testing no other minima were found.

The uniqueness was further investigated by finding the unconstrained minimum of F. A Newton scheme was used for which convergence was very rapid. Solutions were found for M varying from 50 to 100. In all cases F was less than 10^{-20} and h decreased monotonically from 0 to −1, the asymptotic behaviour being $h \sim -1(2\pi x^2)^{-1}$. The behaviour near the origin was closely represented by $h = -4A_0 x^{\frac{1}{2}}$ with $A_0 = 0.44436$.

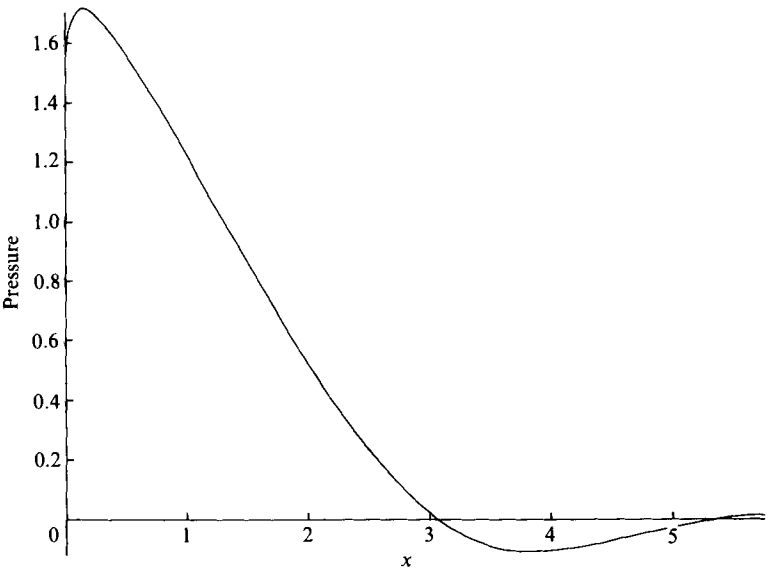

FIGURE 2. Elastic contribution to the non-dimensional cavity pressure as a function of the non-dimensional distance from the crack tip. $M = 110$, $N = 109$, $\epsilon_j = 10^{-9}$.

The dependence on M was tested by comparing solutions obtained to problems (5.1a, b) for increasing values of M to the original solution, holding $N = M-1$ throughout. In all cases the results agreed closely. The computation was also repeated using the modified objective function,

$$\sum_i [h_i^2(p'+1)-1]^2,$$

virtually identical results being obtained.

Finally the accuracy of the integration scheme was checked by repeating the calculations using a composite six point Gauss–Legendre scheme and an adaptive four-point Gauss–Legendre scheme. The values agreed to six significant figures with the original ones.

The shape $h(x)$ and pressure $p(x)$ (obtained by integrating the computed p') are plotted in figures 1 and 2.

6. Applications

In terms of the non-dimensional variables we have found a universal shape for buoyancy-driven fluid fracture. This shape is given in figure 1. The maximum non-dimensional width of the crack is $H = 1.8975$ and this occurs at $X = 1.152$. Since a solution is found only for a single value of the stress-intensity factor the asymptotic width of the fracture is related to the stress-intensity factor by

$$h_\infty = 0.44 \frac{K_{\mathrm{I}}^{\frac{4}{3}}(1-\nu)}{g\Delta\rho\mu}. \tag{6.1}$$

For a specified value of the stress-intensity factor a crack must have the width given by (6.1) if it is to propagate at a constant velocity.

The critical stress-intensity factor K_{c} is a measure of the fracture toughness of the

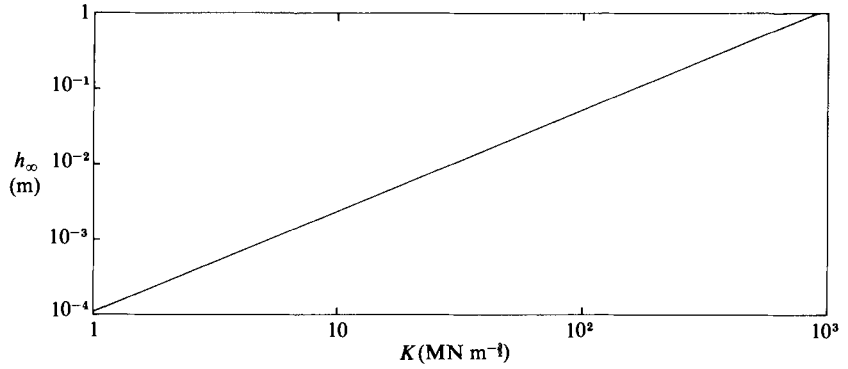

FIGURE 3. Dependence of the asymptotic crack width on the stress-intensity factor.

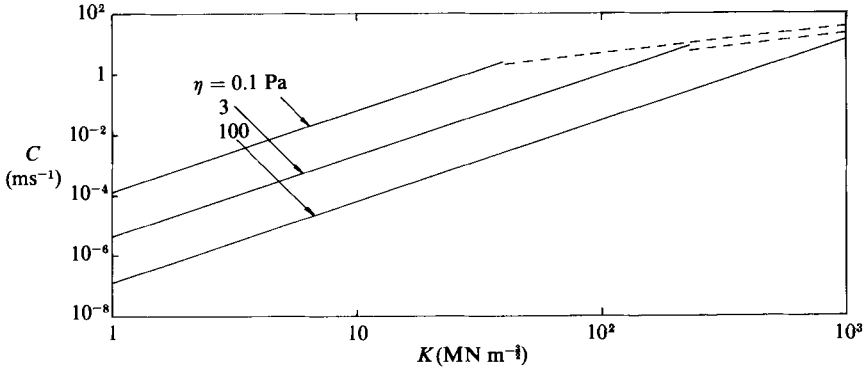

FIGURE 4. Dependence of the propagation speed C on the stress-intensity factor K for several values of the magma viscosity η. ——, laminar; – – –, turbulent.

material. Cracks can propagate at low velocities (about 10^{-4} m/s) by the mechanism of stress corrosion; in this range $K < K_c$. However, when $K = K_c$ crack propagation becomes catastrophic and the propagation velocity may rapidly accelerate to a large fraction of the speed of sound. The value of K_c for a variety of crustal rocks have been obtained in the laboratory. This work has been reviewed by Atkinson (1984). Typical values for crustal rocks lie within the range $K_c = 1$–3 MN m$^{-\frac{3}{2}}$ both for granites and for basalts with some dependence on grain size. A measured value for dunite that is a typical mantle rock is $K_c = 4$ MN m$^{-\frac{3}{2}}$. All these values were obtained at atmospheric pressure. The influence of pressure on the stress-intensity factor is difficult to predict. Schmidt & Huddle (1977) found a factor of four increase at a pressure of 62 MPa for Indiana limestone. Thus it is difficult to specify values of the stress-intensity factor for regions of the crust and mantle where buoyancy-driven magma fracture is occurring.

Taking $\mu = 2 \times 10^{10}$ Pa, $\nu = 0.25$, $\Delta\rho = 300$ kg m^{-3} and $g = 10$ ms^{-2} the asymptotic width h_∞ is given as a function of the stress-intensity factor K in figure 3. From $\bar{h}_\infty^2 = \bar{c}$ the propagation speed c is related to the asymptotic width h_∞ by

$$c = \frac{h_\infty^2 \Delta\rho g}{3\eta_m}. \tag{6.2}$$

Propagation speeds are given as a function of the stress intensity factor in figure 4. Results are given for viscosities $\eta_m = 0.1, 3, 100$ Pa s. This range covers the measured values for a variety of magmas (Kushiro 1980; Persikov 1981). Our laminar analysis

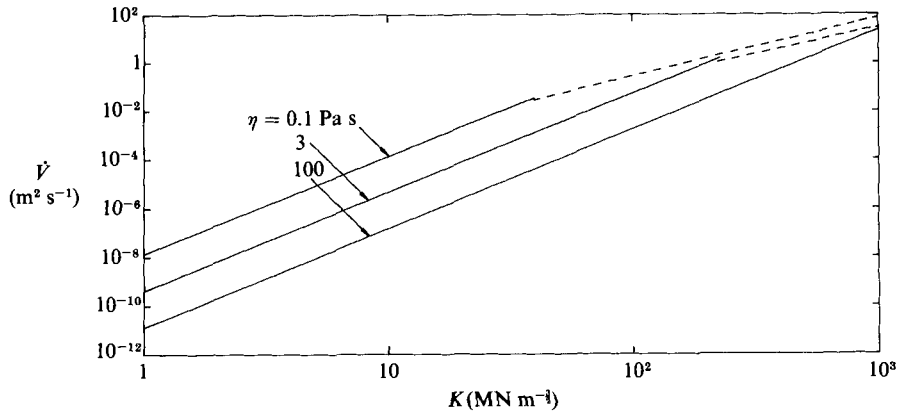

FIGURE 5. Dependence of the volumetric magma flux $\dot{V}$ on the stress-intensity factor K for several values of the magma viscosity η. ——, laminar; – – –, turbulent.

is valid if the Reynolds number $Re = \rho_m c h_\infty / \eta_m$ is less than about 10^3. As an approximation for the turbulent regime we replace (6.2) with the equivalent turbulent relation

$$c = \frac{7.71 h_\infty^{\frac{5}{7}} (\Delta\rho g)^{\frac{4}{7}}}{\rho_m^{\frac{2}{7}} \eta_m^{\frac{1}{7}}}. \tag{6.3}$$

This relation is used to give the propagation velocity in figure 4 if $Re > 10^3$. The corresponding values of the volumetric flow rate $\dot{V} = c h_\infty$ are given in figure 5.

In many cases heavy blocks of solid rock (xenoliths) are entrained in basaltic magma flows. Carmichael *et al.* (1977) have shown that this entrainment implies magma velocities of at least $c = 0.5$ m/s. A variety of studies indicate that basaltic magma migrates vertically at velocities in the range $c = 0.5$–5 m/s. A typical viscosity for a basaltic magma is 0.1 Pa s. From figures 3 and 4 the corresponding range of the stress-intensity factor is $K = 20$–100 MN $m^{-\frac{3}{2}}$ and the range of asymptotic widths is $h_\infty = 5$–50 mm. From figure 5 the corresponding range of flow rates is $V = 0.0025$–0.25 $m^2\ s^{-1}$.

Studies of the Kilauea Iki eruption on the island of Hawaii during 1959–1960 give flow rates of 50–150 m^3/s (Williams & McBirney 1979 pp. 232–233). Taking a flow rate of 100 m^3/s, the range of flow rates given above, $V = 0.0025$–0.25 $m^2\ s^{-1}$, corresponds to crack lengths between 400 m and 4 km. These appear to be reasonable values for the crack feeding the Hawaiian volcano. Although the above comparison appears reasonable, there is conflicting evidence as to whether the flow of magma at the surface represents the flow rate through the lithosphere. The role of shallow magma chambers in storing magma is poorly understood.

7. Conclusions

We have obtained a steady-state solution for a buoyancy-driven fluid fracture. For a specified value of the stress-intensity factor the width and propagation speed of the crack are determined. Thus the flow through the crack is also specified. If the available magma source requires a greater flow, then, presumably, the crack propagation problem will not result in a steady state.

Reasonable values for the crack propagation velocity, flow velocity, and magma flux are obtained if $K \approx 60$ MN $m^{-\frac{3}{2}}$. This is considerably higher than laboratory values obtained at atmospheric pressure ($K = 1$–3 MN $m^{-\frac{3}{2}}$). However, there is

laboratory evidence that K increases with increasing pressure so that $K \approx 60$ MN m$^{-\frac{3}{2}}$ is reasonable for mantle conditions.

It is clear that our solution is only approximately valid for magma migration. An actual crack in the mantle or crust is three dimensional. Also, magma may melt wall rock or it may solidify against the wall rock. Nevertheless, we believe that the calculations given in this paper provide a reasonable approximation for the vertical ascent of magma to the Earth's surface. This mechanism can explain the rapid ascent velocities required for the transport of diamonds to the surface during a Kimberlitic eruption.

This work was supported in part by the Division of Earth Sciences, National Science Foundation, under grant EAR 8318563.

Appendix A. Evaluation of $R(x)$, equation (3.10)

If we define

$$g(x) = h(x) - 1 - 1/2\pi(x^2+1),$$

the remainder term in (3.10) becomes

$$R(X) = \frac{1}{\pi x^2}\left[-\frac{1}{\pi}\int_0^\infty \frac{s^3\,\mathrm{d}s}{(s-x)(s^2+1)^2} + \int_0^\infty \frac{s^2}{s-x} g'(s)\,\mathrm{d}s\right].$$

The first integral in the square bracket can be rearranged as

$$-\frac{1}{\pi(x^2+1)}\int_0^\infty \left(\frac{x}{s-x} + \frac{1-xs}{s^2+1}\right)\mathrm{d}s + \frac{1}{\pi}\int_0^\infty \left(\frac{s}{s-x}\right)\frac{\mathrm{d}s}{(s^2+1)^2},$$

after which integration gives its value as

$$\frac{1}{\pi x}\left(\ln x - \tfrac{1}{2} + O\left(\frac{1}{x}\right)\right),$$

while the second behaves for large x like

$$-\frac{1}{x}\int_0^\infty s^2 g'(s)\,\mathrm{d}s.$$

Integration by parts is permissible since $g = O(1/s^3)$ as $s \to \infty$, giving altogether

$$R = \frac{1}{\pi^2 x^3}(\ln x - \tfrac{1}{2} + 2\pi B) + o\left(\frac{1}{x^3}\right),$$

where

$$B = \int_0^\infty s g(s)\,\mathrm{d}s.$$

Appendix B. Evaluation of $H_n(\psi)$ (equation 4.2)

If we define

$$I_n(\psi) = \left(\frac{1}{\pi}\right)\int_0^\pi \left(\frac{\cos\vartheta - \cos\psi}{\sin\vartheta}\right)\ln\left|\frac{\tan\frac{1}{2}\vartheta + \tan\frac{1}{2}\psi}{\tan\frac{1}{2}\vartheta - \tan\frac{1}{2}\psi}\right|\cos n\vartheta\,\mathrm{d}\vartheta.$$

Then since

$$\frac{\partial}{\partial\psi}\ln|\,| = \frac{-\sin\vartheta}{(\cos\vartheta - \cos\psi)},$$

(i)
$$I_0'(\psi) = \frac{\sin\psi}{\pi}\int_0^\pi \ln|\,|\,\frac{\mathrm{d}\vartheta}{\sin\vartheta} - \frac{1}{\pi}\int_0^\pi \mathrm{d}\vartheta = \tfrac{1}{2}\pi\sin\psi - 1,$$

and since $I_0(0) = 0$, integration gives

$$I_0(\psi) = \tfrac{1}{2}\pi(1-\cos\psi)-\psi,$$

(ii)
$$I_1'-I_0' = \frac{\sin\psi}{\pi}\int_0^\pi \ln|\,|(\tan\tfrac{1}{2}\vartheta)\,\mathrm{d}\vartheta+1.$$

The integral is zero when $\psi = 0$, and can be evaluated by differentiation with respect to ψ:

$$\frac{\mathrm{d}}{\mathrm{d}\psi}\int_0^\pi \ln|\,|(\tan\tfrac{1}{2}\vartheta)\,\mathrm{d}\vartheta = -\int_0^\pi \frac{2\sin^2\tfrac{1}{2}\vartheta}{\cos\vartheta-\cos\psi}\,\mathrm{d}\vartheta = \pi.$$

Therefore,
$$I_1'-I_0' = -\psi\sin\psi+1,$$

whence,
$$I_1 = I_0+\psi\cos\psi-\sin\psi+\psi.$$

(iii)
$$I_2'-I_0' = -\frac{\sin\psi}{\pi}\int_0^\pi \ln|\,|(2\sin\vartheta)\,\mathrm{d}\vartheta+1,$$

and since

$$\frac{\mathrm{d}}{\mathrm{d}\psi}\int_0^\pi \ln|\,|(2\sin\vartheta)\,\mathrm{d}\vartheta = \int_0^\pi \frac{-2\sin^2\vartheta}{\cos\vartheta-\cos\psi}\,\mathrm{d}\vartheta = \pi\left(\frac{\sin 2\psi}{\sin\psi}\right),$$

we obtain after two integrations

$$I_2-I_0 = \tfrac{1}{2}\sin 2\psi.$$

(iv) More generally, for $n > 1$,

$$I_{n+1}'-I_{n-1}' = -\left(\frac{\sin\psi}{\pi}\right)\int_0^\pi \ln|\,|(2\sin n\vartheta)\,\mathrm{d}\vartheta$$

$$\frac{\mathrm{d}}{\mathrm{d}\psi}\int_0^\pi \ln|\,|(2\sin\mathrm{d}\vartheta)\,\mathrm{d}\vartheta = \int_0^\pi \frac{-2\sin n\vartheta\sin\vartheta}{\cos\vartheta-\cos\psi}\,\mathrm{d}\vartheta = \pi\left(\frac{\sin(n+1)\psi-\sin(n-1)\psi}{\sin\psi}\right),$$

so that two integrations give

$$I_{n+1}-I_{n-1} = \frac{1}{n}\left\{\frac{\sin(n+1)\psi}{n+1}-\frac{\sin(n-1)\psi}{n-1}\right\}.$$

In terms of the I_n

$$H_0 = \sec^2\tfrac{1}{2}\psi I_0-2\tan\tfrac{1}{2}\psi = (\pi-\psi)\tan^2\tfrac{1}{2}\psi-\psi\sec^2\tfrac{1}{2}\psi-2\tan\tfrac{1}{2}\psi,$$

$$H_1 = (\sec^2\tfrac{1}{2}\psi)\,I_1 = H_0+2\psi,$$

$$H_2 = (\sec^2\tfrac{1}{2}\psi)\,I_2 = H_0+2\sin\psi,$$

$$H_{n+1}-H_{n-1} = (\sec^2\tfrac{1}{2}\psi)\,(I_{n+1}-I_{n-1}).$$

Appendix C. A linearized solution

For $h(x)$ is close to 1, (3.2) gives

$$p'(x) = -2(h(x)-1)+O(h(x)-1)^2.$$

When the squared term is excluded, substitution for h' in (3.1) gives the linear integro-differential equation

$$p(x) = \frac{1}{2\pi}\int_0^\infty \frac{p''(s)\,\mathrm{d}s}{s-x}. \qquad \text{(C 1)}$$

This equation can be solved as follows by use of the Mellin transform, and the result used to obtain an expression for $h(x)$. We write

$$P(z) = \int_0^\infty x^{z-1} p(x)\,\mathrm{d}x, \tag{C 2}$$

with inverse

$$p(x) = \frac{1}{2\pi \mathrm{i}} \int_{c-\mathrm{i}\infty}^{c+\mathrm{i}\infty} x^{-z} P(z)\,\mathrm{d}z \tag{C 3}$$

where $\mathrm{Re}\, z = c$ lies in the strip of regularity of $P(z)$. Then

$$p''(x) = \frac{1}{2\pi \mathrm{i}} \int_{c-\mathrm{i}\infty}^{c+\mathrm{i}\infty} z(z+1)\, x^{-z-2} P(z)\,\mathrm{d}z, \tag{C 4}$$

and if $z(z+1)\,P(z)$ is regular in the strip $c-2 < \mathrm{Re}\, z < c$ this integral can be written

$$\frac{1}{2\pi \mathrm{i}} \int_{c-1\infty}^{c+1\infty} (z-2)(z-1)\, x^{-z} P(z-2)\,\mathrm{d}z. \tag{C 5}$$

Then since

$$\frac{1}{\pi} \int_0^\infty \frac{s^{-z}\,\mathrm{d}s}{s-x} = x^{-z}(\cot \pi z) \quad (0 < \mathrm{Re}\, z < 1),$$

provided $0 < c < 1$, the right-hand side of (C 5) becomes

$$\frac{1}{2\pi \mathrm{i}} \int_{c-\mathrm{i}\infty}^{c+\mathrm{i}\infty} \tfrac{1}{2}(z-2)(z-1)\, x^{-z} (\cot \pi z)\, P(z-2)\,\mathrm{d}z,$$

which when equated to (C 3) gives the functional equation

$$2P(z) = (z-1)(z-2)(\cot \pi z)\, P(z-2). \tag{C 6}$$

$h(x)$ is given in terms of P by

$$h(x) = 1 - \tfrac{1}{2} p'(x) = 1 + \frac{1}{2\pi \mathrm{i}} \int_{c-\mathrm{i}\infty}^{c+\mathrm{i}\infty} H(z)\, x^{-z}\,\mathrm{d}z, \tag{C 7}$$

say, where

$$H(z) = \tfrac{1}{2}(z-1)\, P(z-1).$$

Therefore $H(z)$ satisfies the functional equation

$$2H(z+1) = z(z-1)(\cot \pi z)\, H(z-1). \tag{C 8}$$

The general solution of this equation satisfying the constraint (C 4) and suitably bounded as $\mathrm{Im}\, z \to \infty$ is given by

$$H(z) = (A + C \cot \tfrac{1}{2}\pi z)\, \Phi(z), \tag{C 9}$$

where A, C are arbitrary constants, and

$$\Phi(z) = 2^{\frac{1}{2}(z-1)} \frac{G(1+\frac{1}{2}z)\, G^2_{\frac{1}{2}}(3+z)\, G(\frac{7}{4}-\frac{1}{2}z)\, G(\frac{5}{4}-\frac{1}{2}z)}{G(2-\frac{1}{2}z)\, G^2_{\frac{1}{2}}(3-z)\, G(\frac{3}{4}+\frac{1}{2}z)\, G(\frac{1}{4}+\frac{1}{2}z)}.$$

Here $G(z+1)$ is the Alexeievski function (Whittaker & Watson 1946 p. 264) which satisfies the functional equation

$$G(z+1) = \Gamma(z)\, G(z), \quad G(1) = 1.$$

$G(z+1)$ is regular throughout the complex plane and has zeros of order n at $z = -n$, $n = 1, 2, \ldots$.

$\Phi(z)$ therefore has simple poles at $z = -\frac{3}{2}, -\frac{1}{2}, 3, 4$.

The factor $\cot \frac{1}{2}\pi z$ introduces additional poles at $z = 0, 2$ and suppresses that at $z = 3$.

The integral (C 7) can now be expanded in terms of the residues at the poles of $H(z)$. Those in $\mathrm{Re}\, z < c$ give the expansion for $x < 1$ as

$$h(x) = 1 + 2C + 2^{\frac{7}{4}}\pi^{-\frac{1}{2}}(A - C)\, x^{\frac{1}{2}} + O(x^{\frac{3}{2}})$$

while those in $\mathrm{Re}\, z > c$ give

$$h(x) \approx 1 - \frac{C}{\pi x^2} - \frac{A}{\pi x^3} + O\left(\frac{1}{x^4}\right) \quad (x > 1).$$

The linearization underlying the equation is not valid at $x = 0$, but if nevertheless the constant C is chosen as $-\frac{1}{2}$ to ensure that $h(0) = 0$, these become

$$h(x) = 2\lambda x^{\frac{1}{2}} + O(x^{\frac{3}{2}}) \quad (x < 1),$$

$$h(x) \approx 1 + \frac{1}{2\pi x^2} - \frac{A}{\pi x^3} + O\left(\frac{1}{x^4}\right) \quad (x > 1),$$

with $\lambda = 2^{\frac{3}{4}}\pi^{-\frac{1}{2}}(A + \frac{1}{2})$. The leading terms are now of the same form as those of (3.6), (3.12) respectively, but the constant a is undetermined. A is related to the integral of h in exactly the same way as for the non-linear problem:

$$\int_0^\infty (h - 1)\, \mathrm{d}x = H(1) = A.$$

This agrees with (4.15).

REFERENCES

Anderson, O. L. 1979 The role of fracture dynamics in Kimberlite pipe formation. In *Kimberlites, Diatremes, and Diamonds: Their Geology, Petrology, and Geochemistry* (ed. F. R. Boyd & H. O. A. Meyer), vol. 1, pp. 344–353. American Geophysical Union.

Anderson, O. L. & Grew, P. C. 1977 Stress corrosion theory of crack propagation with applications to geophysics. *Rev. Geophys. Space Phys.* **15**, 77–104.

Atkinson, B. K. 1984 Subcritical crack growth in geological materials. *J. Geophys. Res.* **89**, 4077–4114.

Carmichael, I. S. E., Nicolls, J., Spera, F. J., Wood, B. J. & Nelson, S. A. 1977 High-temperature properties of silicate liquids: applications to the equilibration and ascent of basic magma. *Phil. Trans. R. Soc. Lond.* A **286**, 373–431.

Delaney, P. T. & Pollard, D. D. 1981 Deformation of host rocks and flow of magma during growth of minette dikes and breccia-bearing intrusions near Ship Rock, New Mexico. *U.S. Geol. Survey Prof. Paper* 1202, 61 pp.

Delaney, P. T. & Pollard, D. D. 1982 Solidification of basaltic magma during flow in a dike. *Am. J. Sci.* **282**, 856–885.

Emerman, S. H., Turcotte, D. L. & Spence, D. A. 1986 Transport of magma and hydrothermal solutions by laminar and turbulent fluid fracture. *Phys. Earth Planet. Int.* **41**, 249–259.

Kushiro, I. 1980 Viscosity, density, and structure of silicate melts at high pressures, and their petrological applications. In *Physics of Magmatic Processes* (ed. R. B. Hargraves), pp. 93–120. Princeton University Press.

Muller, O. H. & Muller, M. R. 1980 Near surface magma movement. *Proc. Lunar Planet. Sci. Conf.* **11**, 1979–1985.

Pasteris, J. D. 1984 Kimberlites: complex mantle salts. *Ann. Rev. Earth Planet. Sci.* **12**, 133–153.

Persikov, E. S. 1981 Viscosity of magmatic melts, as related to some patterns of silicic and mafic igneous activity. *Dokl. Akad. Nauk SSSR* (Earth Sciences Section), **260**, 47–50.

Pollard, D. D. 1973 Derivation and evaluation of a mechanical model for sheet intrusions. *Tectonophysics* **19**, 233–269.

Pollard, D. D. 1976 On the form and stability of open hydraulic fractures in the earth's crust. *Geophys. Res. Lett.* **3**, 513–516.

POLLARD, D. D. & MULLER, O. H. 1976 The effect of gradients in regional stress and magma pressure on the form of sheet intrusions in cross section. *J. Geophys. Res.* **81**, 975–984.

SCHMIDT, R. A. & HUDDLE, C. W. 1977 Effect of confining pressure on fracture toughness of Indiana limestone. *Intl J. Rock Mech. Min. Sci. Geomech. Abstr.* **14**, 289–293.

SECOR, D. T. & POLLARD, D. D. 1975 On the stability of open hydraulic fractures in the earth's crust. *Geophys. Res. Lett.* **2**, 510–513.

SHAW, H. R. 1980 The fracture mechanisms of magma transport from the mantle to the surface. In *Physics of Magmatic Processes* (ed. R. B. Hargraves), pp. 201–264. Princeton University Press.

SPENCE, D. A. & SHARP, P. 1985 Self-similar solutions for elastohydrodynamic cavity flow. *Proc. R. Soc. Lond.* A **400**, 289–313.

SPENCE, D. A. & TURCOTTE, D. L. 1985 Magma-driven propagation of cracks. *J. Geophys. Res.* **90**, 575–580.

STEVENSON, D. J. 1982 Migration of fluid-filled cracks: applications to terrestrial and icy bodies. *Lunar Planet. Sci. 13th*, 768–769.

WEERTMAN, J. 1971 Theory of water-filled crevasses in glaciers applied to vertical magma transport beneath oceanic ridges. *J. Geophys. Res.* **76**, 1171–1183.

WHITTAKER, E. T. & WATSON, G. N. 1946 *A Course of Modern Analysis.* Cambridge University Press.

WILLIAMS, H. & MCBIRNEY, A. R. 1979 *Volcanology.* Freeman–Cooper.